Available online at www.sciencedirect.com

jmr&t Journal of Materials Research and Technology

journal homepage: www.elsevier.com/locate/jmrt

Original Article

Ultrasensitive SERS platform made via femtosecond laser micromachining for biomedical applications

Tomasz Szymborski [a,*], *Yuriy Stepanenko* [a], *Krzysztof Niciński* [a], *Patrycja Piecyk* [a], *Sylwia M. Berus* [a], *Monika Adamczyk-Popławska* [b], *Agnieszka Kamińska* [a,**]

[a] *Institute of Physical Chemistry, Polish Academy of Sciences, Kasprzaka 44/52, 01-224, Warsaw, Poland*
[b] *Department of Molecular Virology, Institute of Microbiology, Faculty of Biology, University of Warsaw, Miecznikowa 1, 02-096, Warsaw, Poland*

ARTICLE INFO

Article history:
Received 24 November 2020
Accepted 19 March 2021
Available online 25 March 2021

Keywords:
Surface-enhanced Raman spectroscopy
SERS
Femtosecond laser
Laser ablation
Candida
Staphylococcus aureus

ABSTRACT

Surface-enhanced Raman spectroscopy (SERS) is a research method in which a lack of cost-effective, versatile platforms with high enhancement factor (EF) is still a major obstacle to its widespread use. The platforms should be also easy to manufacture, stable in time (for weeks or even for months) and manufactured with a highly reproducible method.

We demonstrate SERS platforms based on silicon modified on the surface by laser ablation and covered with SERS-active metal. The substrates were fabricated by a femtosecond laser, thus the method is simple, very fast and creates highly uniform SERS platforms in a large number. The platform was tested with para-mercaptobenzoic acid (*p*-MBA) in terms of sensitivity and reproducibility. The calculated EF was at the level of 10^8 and the standard deviation (SD) gives 7% for 10^{-6} M solution of *p*-MBA based on the intensity of the band at 1073 cm^{-1}. Optimized SERS substrate also exhibits excellent stability for up to six months.

We also give the proof-of-concept of using our platform and, for the first time, the SERS analysis of the most important human opportunistic fungal pathogen *Candida* spp. (*Candida glabrata*, *Candida albicans SN148* and *C. albicans BWP17*). Finally, the chemometric analysis in the form of Principal Component Analysis (PCA) allowed to strain differentiation of *Candida* spp., and to distinguish the studied *Candida species* from Gram-positive bacterial samples with *Staphylococcus aureus*. Our results demonstrate that the proposed SERS platform is a perfect substrate for detection, identification and differentiation between fungal and bacterial pathogens using SERS technique.

* Corresponding author.
** Corresponding author.
E-mail addresses: tszymborski@ichf.edu.pl (T. Szymborski), akaminska@ichf.edu.pl (A. Kamińska).
https://doi.org/10.1016/j.jmrt.2021.03.083

1. Introduction

The amplification of the Raman signal in the surface-enhanced Raman spectroscopy (SERS) is several orders of magnitudes greater than those obtained by classical Raman spectroscopy [1], thus it makes possibility even single-molecule detection [2,3]. Two effects can explain this phenomenon: the electromagnetic and the chemical effect, however, it is considered that the electromagnetic effect is principally responsible for the SERS signal amplification [4,5]. The SERS technique is highly sensitive and selective (each molecule has a unique characteristic spectrum) method and therefore it makes this technique perfect for detection and identification of bacteria, viruses and other pathogens.

Nowadays, the SERS technique is mainly limited by the poor reliability and reproducibility of the recorded SERS signals. Low consistency is strictly related to the difficulty in controlling the homogeneity and stability of the SERS substrates over time. Therefore, the practical biomedical and analytical applications of the SERS technique on a larger scale are still in the hamper [6]. SERS-active substrates can be divided into two, most commonly used in SERS experiments, types: colloidal suspensions [7] and solid substrates. Solid SERS substrates are usually produced by applying nanoparticles to the rough surface or by phase metal deposition, as a result of which a thin layer of plasmonic nanostructures is created [8]. Controlling the deposition of metal on the platform enables to produce a homogeneous material surface structure for a stronger and repeatable SERS signal, which is very difficult to achieve for the colloidal SERS support.

Recently, laser surface texturing has become one of the most advanced techniques to create various types of micro-cavities on the surface. Laser micromachining [9,10] is a process that uses the energy of a laser beam to remove material at the scale of micrometers or millimeters. Surface modification by femtosecond-induced laser ablation has many advantages: the absence of heat affected zone (HAZ), material removal occurs precisely where the laser beam strikes the material and finally, the method does not require the use of clean-room. Additionally, this method can be used for many materials, from polymers and plastics, through the glass, silicon and ending with metals and their alloys [11]. In contrast to picosecond and nanosecond lasers, pulses of the femtosecond laser deliver several TW/cm^2 of power density to the surface of the material. At such high intensities, interaction between the laser pulse and material initiates several processes such as ablation, shockwave, and ripple formation, which are not reachable for low-intensity laser pulses.

One of the most promising application of the laser-textured surfaces are SERS-active platforms. The laser micromachining via laser ablation for SERS applications was already demonstrated in several scientific articles. Hamad et al. [12] reports the process of preparation of reproducible SERS platforms using femtosecond laser ablation of silicon immersed in acetone. After the ablation process, layers of Ag/Au alloy nanoparticles were deposited. A femtosecond laser with a wavelength of 800 nm, pulse duration of 50 fs and frequency of 1 kHz was used for the ablation process. Reproducible and amplified SERS signals were obtained for methylene blue (MB), 2,4-dinitrotoluene (DNT) and 5-amino-3-nitro-1,2,4-triazole (ANTA). Saikiran et al. [13] sputtered the gold layers of various thicknesses onto the silicon semiconductor substrates obtained via femtosecond laser (wavelength of 800 nm, repetition of 1 kHz and duration of laser pulse was approximately 110 fs). They presented the reproducible SERS spectra of the crystal violet (CV) molecules. Diebold et al. [14] reported the silicon platforms for the SERS technique, which was made using a femtosecond laser, on which a silver layer was then thermally deposited. The parameters of the femtosecond laser used were: wavelength 800 nm, pulse duration 100 fs, repetition frequency 1 kHz. The amplification of the Raman signal for the given platforms was proved for 4-mercaptobenzoic acid solution. Wang et al. [15] described the SERS-based detection using a low-adhesive superhydrophobic substrate. Silicon was subjected to laser ablation using a titanium-sapphire laser with a pulse duration of 35 fs and a wavelength of 800 nm, and then a silver layer with a thickness of 60 nm was sputtered on to the prepared silicon surfaces by the PVD method. The enhancement factor of the fabricated platform was determined to be 6×10^6 and this substrate was subsequently applied to the detection of pesticides and environmental pollutants.

Until now, femtosecond treated silicon substrate has not been optimized for SERS–based biomedical and analytical analysis. We intended to fabricate the ultrasensitive plasmonic nanostructures via femtosecond laser micromachining, which encounter all spectroscopic requirements for such applications, e.g.: (i) metal nanoparticles with regular structures on the surface, (ii) the repeatable signal and its amplification within the entire surface, (iii) long-term stability of the obtained structures - at least several weeks (the active layer insensitive to changes in humidity, temperature or lighting), (iv) high enhancement factor (up to 10^8) and (v) high purity. We have also demonstrated the SERS analysis of *Candida* spp.: *Candida glabrata, Candida albicans SN148 and C. albicans BWP17*, the most important opportunistic human, fungal pathogen that normally exist in oral mucosa, gastrointestinal tract, genitourinary system, vagina and on the skin. Additionally, the performed chemometric analysis allowed us to distinguish the studied *Candida* species from Gram-positive bacterial samples with *Staphylococcus aureus*.

We proposed a new type of SERS platform made with a femtosecond laser. The method is based on the modification of the surface of silicon with a femtosecond laser beam, and as a result, the ablation process makes the surface of the silicon highly uniform. After sputtering of the thin layer of silver, the SERS platform enhances the Raman signal with a factor of over 10^8. The proposed method is fast, cost-effective (involves only silicon and a thin layer of silver) and offers a SERS platform with high stability and uniformity. In our paper, we demonstrated the protocol of making platform, its optimization process (with *p*-MBA molecule as a model molecule) and we give a proof-of-concept: we measure yeast *Candida* spp. and bacteria *S. aureus* with the SERS technique. The proposed platform can be used in a wide spectrum of applications, from the detection of analytical samples to clinical samples from biofluids.

2. Materials and methods

2.1. Materials

As a base material of SERS platforms, we used polished silicon wafers (100 ± 0.3 mm in diameter and 525 ± 25 μm in thickness) manufactured via Czochralski method at the Institute of Electronic Materials Technology (ITME), Warsaw, Poland. Silicon wafers were *p*-type doped, with crystal orientation <100> and resistivity of 1–30 Ω cm. They were hermetically sealed at ITME and opened prior to use at the Institute of Physical Chemistry of the Polish Academy of Sciences (IPC PAS).

Para-mercaptobenzoic acid (*p*-MBA) was a chemical compound used as a standard for platform optimization. For the preparation of 10^{-6} M solution, we used *para*-mercaptobenzoic acid with purity 99% (MOLEKULA, Poland) and ethanol with purity 99.8% (POCH, Poland).

The source of *Candida* species and S. *aureus*, used culture medium and other materials, are described in Section 2.6.2. Water with resistivity over 18 MΩ purified with Milli-Q plus 185 system was used in all experiments.

2.2. Femtosecond laser

We used a femtosecond fiber laser source based on the chirped pulse amplification (CPA) technique delivering laser pulses of a duration of 300 fs to the working region. The key component of the amplifier is a PM NPE based environmentally stable fiber oscillator [16] seeding a two-stage fiber amplifier that employed an ytterbium-doped photonic crystal fiber (rod) in the final booster stage. Parameters of each of the amplification stages were numerically simulated and optimized for the system efficiency using the modified pulse propagation algorithm developed in [17]. The maximum energy of the pulses available at the central wavelength of 1030 nm was 50 μJ, with the pulse repetition frequency fixed at 300 kHz. The linearly polarized beam was delivered to a computer-controlled vertically adjustable sample-holding platform through a galvanometric scanner and focusing optics with the focal length of $f = 163$ mm. The resulting beam focal spot diameter was 60 μm measured at the intensity level of $1/e^2$. The Gaussian profile of the laser beam and the corresponding diameter is shown in Fig. S1.

2.3. Sputtering of silver via PVD method

To cover the surface of modified silicon with a thin layer of silver we used the Physical Vapor Deposition (PVD) technique. The process was performed with a PVD magnetron sputtering device (Quorum, Q150T ES, Laughton, UK). The silver target was obtained from Mennica Metale Szlachetne (Warsaw, Poland). The target diameter was 58 mm, with a thickness of 0.25 mm. The purity of the silver, according to specification, was 4 N. The vacuum during the silver sputtering was on the level of 10^{-2} mbar, whereas the sputtering current was 25 mA. The embedded quartz microbalance controlled the thickness of the sputtered layer. After the deposition process, the SERS platforms were placed into a sterile Petri dish and stored in an inert gas atmosphere.

2.4. Raman measurements and collecting of the spectra

Measurements were carried out with a Renishaw inVia Raman system (Wotton-under-Edge, Gloucestershire, UK) and Bruker BRAVO handheld spectrometer.

Renishaw inVia Raman system was equipped with a 785 nm diode laser. The light from the laser was passed through a line filter and focused on a sample mounted on an X–Y–Z translation stage with a 20 × microscope objective, NA = 0.25. The beam diameter was approximately 2.5 μm. The microscope was equipped with 1200 grooves per mm grating, cutoff optical filters, and a 1024 × 256 pixel Peltier-cooled RenCam CCD detector, which allowed registering the Stokes part of Raman spectra with 5–6 cm^{-1} spectral resolution and 2 cm^{-1} wavenumber accuracy. The experiments were performed at ambient conditions using a back-scattering geometry. The Raman shift range has been set from about 600 cm^{-1} to 1075 cm^{-1}, because there are interesting *p*-MBA bands in this area. The exposure time was 1 secondand 1 accumulation with the power of the laser set to 10% (equal to 5 mW or less).

Processing the spectra was done with OPUS software, ver. 2012 (Bruker Optic Gmbh Germany). All the spectra were smoothed (5 points), baseline corrected (Concave rubberband correction, number of iterations: 6, number of baseline points: 6) and normalized using 'Min-Max normalization'. The spectra were averaged form about 25–30 single measurements.

Bruker BRAVO handheld spectrometer was equipped with Duo LASER (700–1100 nm) and an integrated CCD camera. The power of the laser was, according to the producer, lower than 100 mW. The spectrometer was connected with a laptop equipped with OPUS software, ver. 2012 (Bruker Optic Gmbh Germany). The software allowed the acquisition of the spectra and initial preprocessing of the obtained data. For each *Candida* and bacteria strain the spectra were recorded in the range 550–1700 cm^{-1}. The time of completing a single spectrum was 18 s (time: 6000 ms, the number of accumulation: 3). The OPUS software, ver. 2012 (Bruker Optic Gmbh Germany) was used for processing of the spectra. All the spectra were smoothed (5 points), baseline corrected (Concave rubberband correction, number of iterations: 6, number of baseline points: 6) and normalized using 'Min-Max normalization'. The spectra were averaged form about 40 single measurements.

2.5. Morphology and analysis of the surface

The morphology of the surface was examined via Scanning Electron Microscopy (SEM). Additionally, we have used optical microscopy to perform a preliminary qualitative assessment of the surface of the silicon.

Scanning Electron Microscopy (SEM) was used to visualize the morphology of silicon:

i) after modification with femtosecond laser and
ii) after modification with femtosecond laser and sputtering of the silver layer via the PVD method.

SEM observations were performed under high vacuum using the FEI Nova NanoSEM 450 (Hillsboro, OR, USA). All the samples were observed in Secondary Electrons (SE) mode and

the accelerating voltage was 5 kV. The samples of silicon were attached to SEM stabs with carbon tape or silver paint and observed without any additional layer of gold or carbon on the surface.

Local analysis of the chemical composition of silicon was performed by XPS spectroscopy. The analysis was performed in the area of 500 μm^2 with the PHI 5000 VersaProbe (Scanning ESCA Microprobe ULVAC-PHI) spectrometer. The source of excitation was monochromatic X-rays with energy hn = 1486.6 eV (AlKa), with parameters: voltage 15 kV and power 25 W. The review and high-resolution XPS spectra were recorded with energy matching function respectively: 117.4 eV and 23.5 eV.

X-Ray Diffraction (XRD) was used to assess the size of the silver nanocrystals on the surface of the modified silicon. The structure of the silicon and parameters of the PVD process leads to a change in the size of silver crystals. Spinning samples were analyzed with the Empyrean 2 (PANalytical) X-ray Diffraction System. For measurements, we used radiation line Cu Kα1 (KL3) equal 1.540598 Å and the analyzed reflex Ag (111) was at angle $2\theta = 38.116^{\circ}$.

2.6. p-*mercaptobenzoic acid and biological samples*

2.6.1. p-*mercaptobenzoic acid* (p-*MBA*)

For the preliminary measurements and optimization of the platform *p*-mercaptobenzoic acid (*p*-MBA) was used. The test platform was silicon with dimensions 3 mm × 3 mm, subjected to laser ablation and sputtering of silver. Afterward, it was immersed in an ethanol solution of *p*-MBA at a concentration of 10^{-6} M and volume 2 ml for 24 h. The vial with the *p*-MBA solution and the SERS platform was placed on the laboratory cradle to mix the solution evenly and gently over the platform. After 24 h, the platform was removed from the solution, attached to the laboratory slide with double-sided tape and left for 5 min at room temperature to evaporate the remaining solution. After this time, it was placed on the microscopic table of a Renishaw Raman spectrometer.

2.6.2. *Measurement of bacteria and* Candida *species*

We have used bacteria and *Candida* yeast to test our SERS platform against biological samples. The *Candida* yeast was obtained from the Faculty of Biology of the University of Warsaw (Warsaw, Poland), and the bacteria, *S. aureus* was obtained from the National Drug Institute (Warsaw, Poland).

To grow *Candida* species, we have used two different types of culture medium: chromogenic medium (chromID Candida agar, CAN2, Biomerieux) and YPD (Yeast extract Peptone Dextrose, Becton Dickinson) agar, whereas to grow *S. aureus* we used Columbia blood agar medium. Both microorganisms grew at 37 °C in aerobic conditions for 24 h.

Each tested colony of microorganisms was selected via inoculation loop from the culture medium and transfer into 100 µl of 0.9% NaCl solution. The solution of bacteria or yeast cells was centrifuged for 3 min at 1070×*g*. The supernatant was discarded and the next portion of the saline solution was added and then centrifuged once again. This process repeats 3 times in order to obtain purified cells. After all, the pellet was re-suspended in 10 µl of NaCl solution and mixed. Finally, the droplet with a volume of 2 ± 0.5 µl was placed onto the SERS platform, which was afterward attached to the laboratory slide with double-sided tape and left for 5 min at room temperature to evaporate the remaining solution. After this time, a laboratory slide with the SERS platform was assembled in the holder table of a Bruker BRAVO spectrometer.

3. Results and discussion

3.1. *Preparation of the SERS platform*

The procedure of preparation of the SERS platform is demonstrated in Fig. S2 and described in details in ESI (S1). The whole process consists of three main steps: (i) initial preparation of the silicon, (ii) modification of the surface and (iii) sputtering of the SERS-active layer of metal. Shortly, in the first step we mechanically cut the silicon into small squares. In the second, main step, we have used femtosecond laser for surface modification of the silicon. The modification develop the surface roughness in nano- and micro-level, increasing the possible places where 'hot-spots' could occur. In the last step, the modified silicon was stoppered with SERS-active metal, i.e. 100 nm layer of silver.

3.2. *Modification of the silicon: optimization of the process of ablation*

The process of modification of silicon is based on the phenomenon of laser ablation: complex physico-chemical processes induced by incident laser radiation, as a result of which the material layer is removed from the surface. For ablation, the energy density of laser radiation (fluence, defined as the energy of a single pulse divided by area of the laser beam) must be in the order of 0.1–10 J cm^{-2} [18,19]. The dynamics of material removal from the surface and its nucleation on the surface of the silicon are crucial for the generation of nanoparticles, which creates a highly developed structure on the substrate [20]. Laser ablation significantly reduces the thermal degradation of the material and allows to remove fragments of material with good accuracy. The process is well suited for the precise machining of plastic materials [21] as well as semiconductors, metals, alloys, ceramics [22,23], and even bioresorbable polymers for the fabrication of medical implants [24]. High precision of processing with laser ablation ensures mutual coupling of material parameters and laser, therefore it is essential to find the proper parameters of laser and parameters of the laser beam for effective modification of the surface of the material.

The depth of the ablation layer depends on the property of: i) optical (laser radiation absorption depth) and thermal (coefficient heat conduction, temperature diffusion coefficient and heat of vaporization) properties of the material, and ii) laser beam parameters: laser wavelength (λ), the average power of the laser beam, fluence and or energy density in a single pulse (E_d), repetition rate (*f*), focus conditions, speed translation of the processed sample (υ), number of repetitions (here, number of ablation layers, *n*).

In these studies, the work parameters of the femtosecond laser have been optimized in order to achieve the best spectroscopic properties of the fabricated platform, i.e., the

highest enhancement factor (EF) measured for the layer of *p*-MBA (10^{-6} M) on the surface of modified silicon with a sputtered layer of silver.

3.2.1. *Influence of the energy and fluence of the laser on the morphology of silicon*

In the first experiment, different energies (*E*) of the femtosecond laser were used to create the SERS platforms. The energy (*E*) of the laser impulse is proportional to fluence (E_d), as fluence is energy divided by the area of the laser beam, *S* (which is constant through all experiments and equal 2.8×10^{-9} m^2). Application of 100% relative energy (E_r) corresponds to driving voltage (*U*) of 5 V and, as a result, laser pulse energy of 50 μJ. Based on these relationships, a dependency diagram was created: the energy of the laser beam (*E*) and relative energy (E_r) as a function of the applied driving voltage. As can be seen in Fig. 1, the area 'A' (relative energy: 0–32%) is below the ablation threshold for the silicon, thus the change of the surface of silicon is not present and the surface of the silicon remains intact. The area 'B' (relative energy in the range from 32% to 42%) determines the energy capable of initiating the ablation process. In the area 'C' (relative energy above 42%), the increase in the control voltage did not result in changes on the silicon surface compared to the voltage value from area 'B'. For this reason, it was decided to conduct precise experiments using the parameters of fluence in area 'B' (see Fig. 1b).

To assess the impact of laser energy and fluence on the morphology of the silicon, we performed a series of experiments on 3 mm × 3 mm silicon squares prepared by the procedure described in Section 3.1. The relative energy of the laser was varied between 32% and 42% (in 1% steps) and lastly, energy of 100%, in order to check the correctness of the assumption, that there is no influence of E_r above 42% on Raman signal amplification. The laser fluence was calculated for each *E* rate by dividing the energy by the area of laser beam S, i.e., 2.8×10^{-9} m^2.

During the preparation of the SERS platforms, the fluence of the femtosecond laser was variable, whereas the following parameters remained constant: distance of scanning lines (*d*) 30 μm, scanning speed (*v*) of the laser beam on the silicon substrate equal 1.5 m/s. We decided to lead the scanning lines parallel and perpendicular (one ablation layer composed of lines arranged in parallel with respect to each other, or two layers with mutual perpendicular orientation) to check which circuit will guarantee a stronger amplification of the Raman signal. The precise values of driving voltage (*U*), the energy of the laser pulse (*E*), relative energy (E_r), and fluence (E_d) are demonstrated in Table S1. Finally, a 100 nm layer of silver was sputtered on each of these platforms.

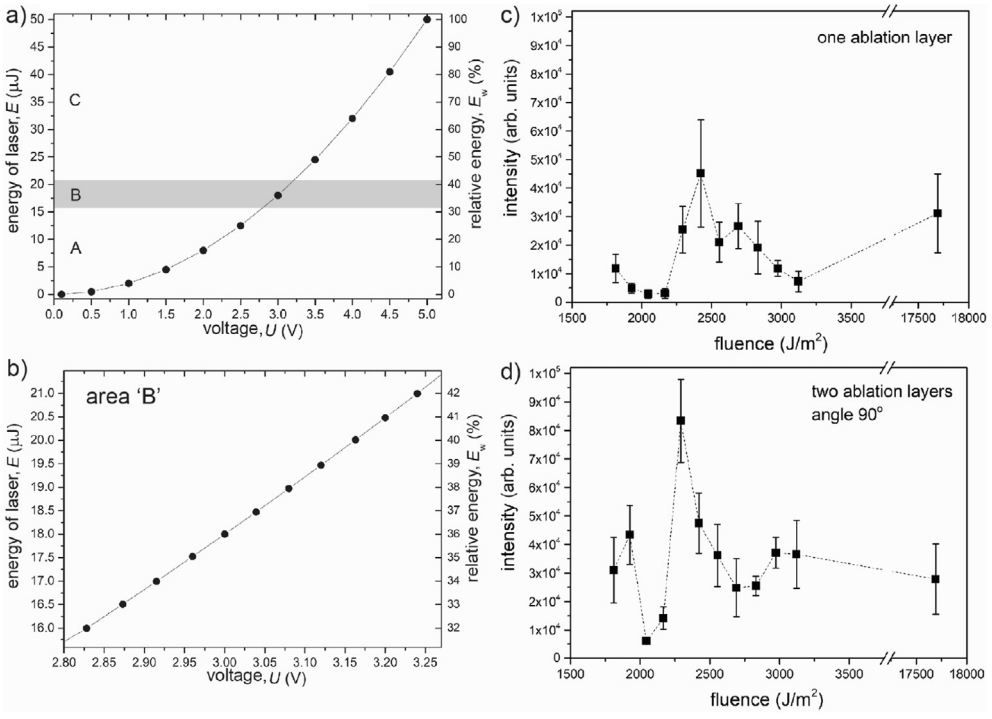

Fig. 1 – Energy (*E*) and corresponding relative energy (E_r) of femtosecond laser as a function of applied driving voltage (*U*): (a) from 0.0 V to 5.0 V, i.e., full range of the driving voltage. The maximum value of voltage is equal to energy 50 μJ. The dependency between energy and voltage is given by $E \propto a \cdot U^2$, where $a = 2$. Three areas of laser operation have been defined as 'A', 'B' and 'C'. (b) area 'B' (between 16.0 μJ and 21 μJ), where the change of the pulse energy influences the ablation process, The average intensity of the 1071 cm^{-1} band of *p*-MBA adsorbed on SERS platform with a different pattern of ablation layers: (c) one ablation layer with laser scanning lines parallel to each other with the distance *d*, and (d) two ablation layers (in both layers, laser scanning lines parallel to each other with the distance *d*), with the orientation of 90°. The detailed scheme of both patterns are demonstrated in Figs. S3–S5.

Then, the platforms were submerged in *p*-MBA EtOH solution for 24 h and afterward were measured according to the procedure described in Sections 2.4 and 2.6.1. A band at about 1071 cm^{-1} was selected as a characteristic marker band to compare the results from SERS platforms obtained with varied parameters. The whole SERS spectra of *p*-MBA from 450 cm^{-1} to 3200 cm^{-1} was presented in ESI, Fig. S6.

Thus, Fig. 1c and d demonstrate the averaged intensity of this band as a function of fluence. For the optimization of the laser pulse energy and its fluence, 24 SERS platforms were manufactured: 12 of them with a parallel arrangement of scanning lines (single ablation layer) and 12 with a perpendicular arrangement of scanning lines (double ablation layers). Each of the sets of platforms was manufactured using the same value of fluence, described in detail in Table S1. This allowed to compare results for the same value of fluence, yet a different number of ablation layers (one versus two). The summary of the obtained results is shown in Fig. 1c and d. For most of the femtosecond laser fluences used, the intensity of the Raman signal for *p*-MBA is higher when scanning lines are arranged perpendicularly (Fig. 1d). The highest intensity of the *p*-MBA band was recorded using fluence equal 2293 J m^{-2} for a platform with double ablation layers and 2422 J m^{-2} for a platform with a single ablation layer. It has also been observed that for both cases the maximum intensity of the signal is for fluence between 2200 and 2500 J m^{-2}, and the mean intensity of the *p*-MBA band decreases out of this range. The comparison of the intensity of *p*-MBA band recorded for platform prepared with the maximum value of fluence (E_r = 100%) shows that in both cases, the intensity is lower than obtained with fluence in the range of 2200 and 2500 J m^{-2}. For this reason, using the maximum value of fluence for the preparation of the SERS platform has no justification in results.

The highest value of the intensity of the *p*-MBA ban was observed for the double ablation layer case for fluence equal 2293 J m^{-2}. For this value, we will receive the highest EF, therefore this value was used in the subsequent stages of optimization of the SERS platform preparation via femtosecond laser ablation.

3.2.2. *Ablation pattern on the surface of the silicon*

For the selected optimal fluence (2293 J m^{-2}), further experiments were conducted. The influence of the ablation pattern in the form of scanning lines layered with different mutual orientations on the intensity of the Raman signal has been examined. The two simplest arrangements, tested in previous experiments, are shown in Figs. S3a and S3b. Additionally, we designed patterns with three (Fig. S3c), four (Fig. S3d) and five ablation layers (Fig. S3e). The prepared silicon surfaces were covered with a layer of 100 nm silver and immersed in the *p*-MBA solution, then the spectra were collected in the same way as previously. The results are presented in Fig. S3f, where the mean intensity of 1071 cm^{-1} band of adsorbed *p*-MBA is plotted against the number of ablation layers. Based on the data presented in Fig. S3f, it can be concluded that the platform with two ablation layers mutually arranged at the angle 90° has the highest average signal intensity Raman for *p*-MBA. Introducing more ablation layers (e.g., 3, 4, or 5) leads to a decrease in the intensity of the *p*-MBA signal. The summary of recorded Raman intensities are demonstrated in Table S2.

All platforms were prepared using fluence equal to 2293 J m^{-2}, and according to Fig. S3f, the two ablation layers are optimal. For this reason, in all further experiments, we used fluence of 2293 J m^{-2} and two perpendicular ablation layers as a base for further optimization.

The detailed schemes of the preparation of the SERS platform based on four and five ablation layers are presented in ESI (see Figs. S4 and S5).

3.2.3. *Scanning speed and distance between scanning lines of the laser beam*

Other optimized parameters of the process were:

i) the scanning speed (*v*) of the laser beam on the surface of the silicon and
ii) the distance between scanning lines (*d*) of the laser beam scanning the silicon substrate. Distance *d* between scanning lines of the laser beam is defined as a distance between the maximum intensity of energy of adjacent laser beams. The illustration of the parameter *d* is shown in Fig. S3b.

During these experiments, the platforms were fabricated using the laser fluence of 2293 J m^{-2} and the pattern of two perpendicular ablation layer.

Firstly, the scanning speed was varied from 0.1 m/s up to 3.5 m/s at different intervals. As can be seen in Fig. 2a, the most significant change in the intensity of *p*-MBA is recorded for scanning speed between 1 m/s and 2 m/s. Therefore, in this range, we performed more experiments to get a detailed view of the dependency between the intensity of scanning speed.

Prepared platforms were sputtered with a 100 nm layer of silver via the PVD process and immersed in the *p*-MBA solution. The intensity of the band at 1071 cm^{-1} from the averaged spectrum for a given platform made with different scanning speed is presented in Fig. 2a. The strongest signal appears for the use of a femtosecond laser scanning speed of 1.5 m/s, therefore this value will remain constant in the subsequent stages of optimization of the process of laser ablation.

Secondly, we optimized the distance *d* between the scanning lines at the surface of the silicon. The laser parameters, selected in the previous experiments, remain constant: two perpendicular ablation layers, fluence equal 2293 J m^{-2} and scanning speed on the silicon substrate: 1.5 m/s. Platforms with the previously selected parameters and the distance of the scanning lines from the range of 10 μm–120 μm were prepared. After that, 100 nm of silver was sputter, and the platforms were immersed in the *p*-MBA solution. The averaged intensity of 1071 cm^{-1} *p*-MBA band and a function of the distance between laser lines are demonstrated in Fig. 4b. Platforms with the distance of laser scanning lines greater than 40 μm are characterized by a much lower average intensity of the *p*-MBA band than these where the distance was in the range of 10–40 μm. The highest value of the band intensity was obtained for the distance of 30 μm, and this value was optimal and used in the next experiments.

3.2.4. *Thickness of the layer of silver*

For all previously prepared silicon surfaces after laser ablation, 100 nm of silver was sputtered using the PVD technique.

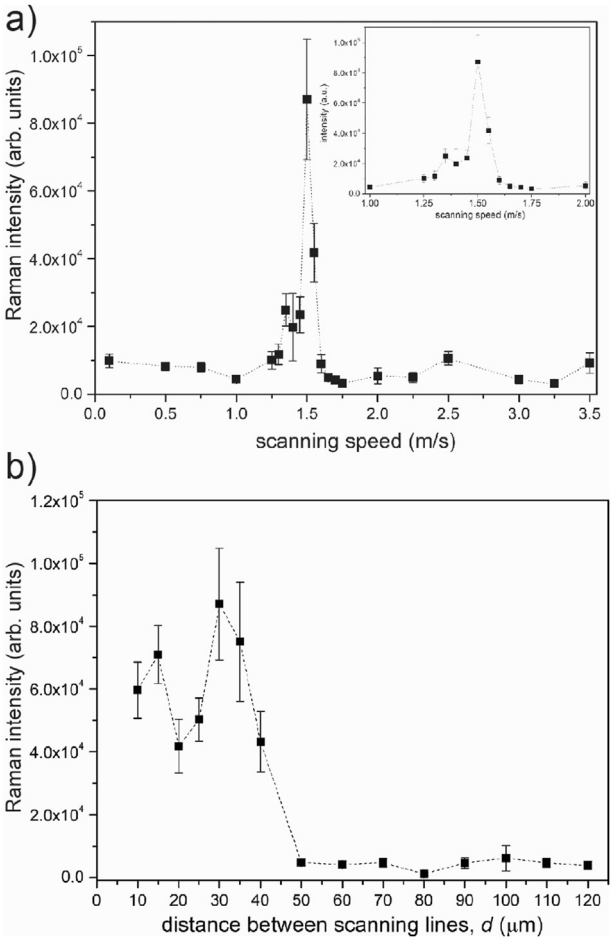

Fig. 2 – (a) The averaged intensity of the 1071 cm^{-1} band of *p*-MBA adsorbed on the surface of SERS platforms made with a different scanning speed of the beam of the femtosecond laser. The inset demonstrate in details range between 1.0 m/s and 2.0 m/s. (b) The average intensity of the 1071 cm^{-1} band of *p*-MBA (10^{-6} M) adsorbed on the SERS platform as a function of the distance, *d*, between scanning lines of the laser beam.

It is known that not only silver can be used in the SERS technique to amplify the Raman signal. For this purpose, we decided to check the dependency of the Raman signal amplification on the thickness of the metal layer as well as metal alloy composition. We have compared silver (99.99%) and an Ag/Au alloy containing 70% of Ag and 30% of Au.

The parameters of the femtosecond laser to produce a rough silicon surface were: the arrangement of scanning layers: perpendicular, fluence, $E_d = 2293\ J\ m^{-2}$, scanning speed of silicon substrate $v = 1.5$ m/s, and distance between the scanning lines $d = 30$ μm. Silver or Ag/Au alloy was sputtered on the prepared platforms in thickness from 10 nm to 100 nm with a difference of 10 nm. The results (the mean intensity of 1075 cm^{-1} band of *p*-MBA) are presented in Fig. S7. Also, the summary of recorded Raman intensities and calculated Enhancement Factors are revealed in Table S2.

Fig. S7 shows that the use of 50 nm and 100 nm layer of silver is associated with obtaining the highest amplification of the Raman signal of the *p*-MBA. When applying a layer of metal below 50 nm, no strong signal amplification was observed. For the thickness of silver equal to 60, 70, 80 and 90 nm, the mean intensity of the 1075 cm^{-1} band is significantly less than for 50 or 100 nm. The best result was obtained for the thickness of the metal layer equal to 100 nm. When using the Ag/Au alloy, the obtained Raman signal was definitely lower than for platforms sputtered with 50 nm or 100 nm layer of silver. The best intensity for the 1071 cm^{-1} *p*-MBA band was obtained for sputtering of 100 nm of silver on the prepared silicon surface.

3.3. *Morphological characterization of SERS platform*

The morphology of the surface of the platform plays a significant role in the SERS technique. To obtain a high enhancement factor, the SERS platform should possess a uniform roughness and the size of nanoparticles on the surface should be below 100 nm. An important issue during the process of ablation is oxidation and possible contamination from the air. For this reason, we used Scanning Electron Microscopy (SEM) to characterize the morphology of the surface of the silicon, before and after sputtering the layer of silver. We have used X-ray Diffraction (XRD) to calculate the size of silver crystallites on the surface and, finally, the X-ray Photoelectron Spectroscopy (XPS) to examine the chemical composition of the sample surface.

3.3.1. *Scanning Electron Microscopy*

Fig. 3 presents the morphology of the silicon platform after ablation with femtosecond laser pulses of different fluence, as well as the comparison of the structure of the SERS platforms with a different number and arrangement of scanning lines. The platforms were prepared with the following constant parameters: double perpendicular ablation layers, the distance between the scanning lines $d = 30$ μm and the thickness of the silver layer was set to 100 nm. For experiments with variable fluence, the scanning speed v of silicon substrate was set to optimal, i.e., 1.5 m/s, whereas for experiments with variable scanning speed v the fluence was set to optimal, i.e., $E_d = 2293\ J\ m^{-2}$.

The results for fluence indicate that the roughness and surface development strongly depends on applied fluence. For fluence 1812 J m^{-2}, i.e., the threshold fluence, where the process starts to occur, we observe the area where the ablation does not progress, or the level is too small to observe via SEM. The sputtering with silver demonstrate (Fig. 3a2) that the surface is not uniform, and this observation correlates with the low intensity of the *p*-MBA band recorded in previous experiments. Substrates after laser ablation with fluence 2293 J m^{-2} and 3121 J m^{-2} demonstrate higher surface development and roughness. The structure after sputtering with a 100 nm layer of silver is uniform, especially for the fluence 2293 J m^{-2}, which is in a good agreement with previous results demonstrating that the intensity of *p*-MBA for fluence 2293 J m^{-2} is the most optimal.

The results for different scanning speeds are demonstrated on the right column of Fig. 3. Three different scanning speeds are depicted in each case for two different magnifications. In this case, no surface with a layer of silver is demonstrated. It can be noticed that for 0.5 m/s the structure is non-uniform,

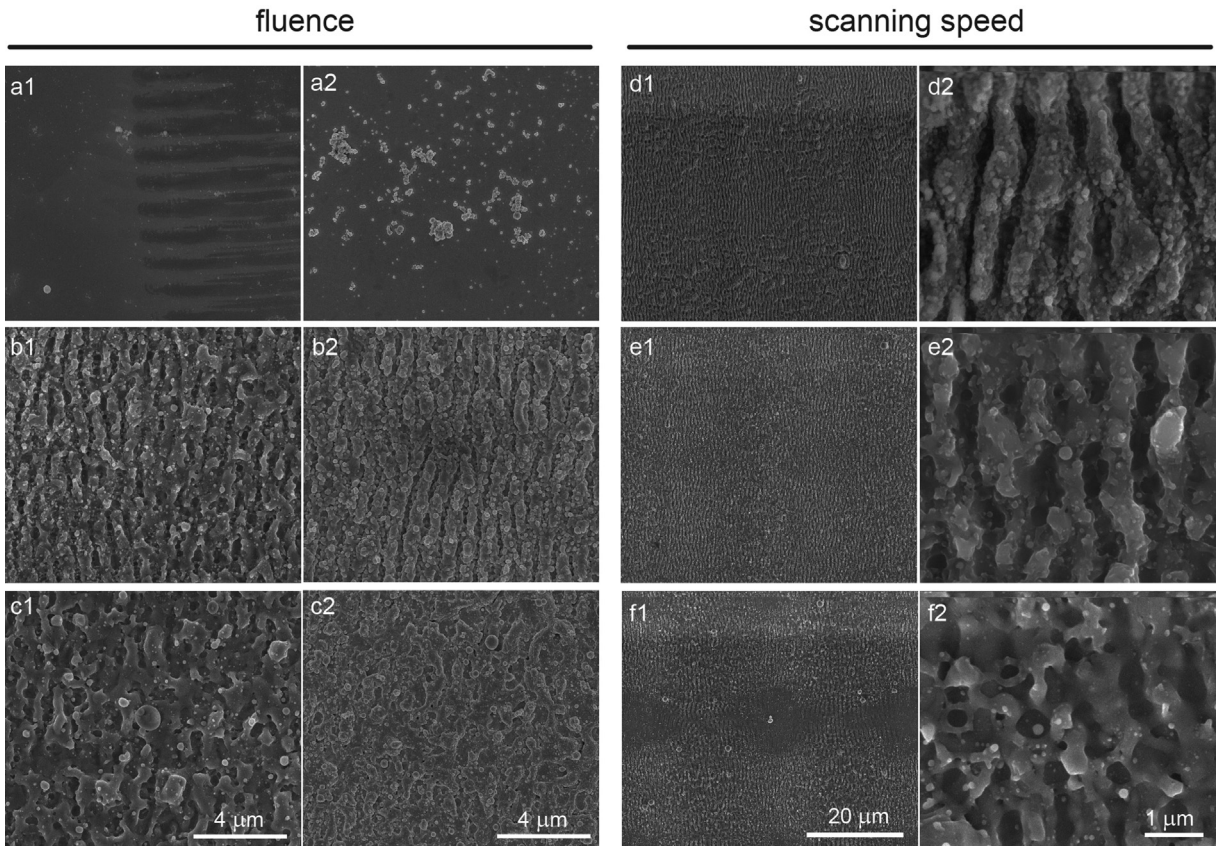

Fig. 3 – On the left column, morphology of the surface of silicon after laser ablation with different energy demonstrated as a fluence for raw surface (a1, b1, c1) and surface with 100 nm Ag layer (a2, b2, c2). Corresponding relative energy (E_r) and fluence (E_d) are: a1–a2) 32% – 1812 J m^{-2}, b1–b2) 36% – 2293 J m^{-2} and c1–c2) 42% – 3121 J m^{-2}. On the right column, morphology of the surface of silicon after laser ablation with different scanning speed v, for two magnifications for raw surface (right). The scanning speed are: d1–d2) 0.5 m/s, e1–e2) 1.5 m/s, and f1–f2) 2.5 m/s.

there are areas of agglomerates of silicon with the size of 1–2 μm on the modified surface. The higher magnification reveals that there is a wide range of the size of silicon nanoparticles. For this reason, the structure with sputtered silver is not uniform and as a result, the enhancement factor will be lower than for uniform surface.

The more uniform surface can be seen for 1.5 m/s and 2.5 m/s, however, for 2.5 m/s we observe at higher magnification higher roughness and a wide range of the size of silicon nanostructures. The results for scanning speed are in good agreement with *p*-MBA experiments: the higher intensity of the *p*-MBA band was recorded for 1.5 m/s, which is a result of uniform structure, both at micro- and nano-scale.

Additionally, in Supplementary Materials, we have presented the influence of the silicon surfaces after laser ablation with a 100 nm Ag layer using different orientation and number of ablation layers (Fig. S8), distance *d* between scanning lines (Fig. S9), and variable thickness of the metal layer (Fig. S10) on the platform after laser ablation on the morphology of obtained SERS platform.

3.3.2. *XPS and XRD analysis of the surface*

XPS analysis was conducted for sample after 1 month and 5 months old. The analysis revealed in both cases distinct bands corresponding to silicon (described as Si 2s and Si 2p) and oxygen (about 1s and O 2s). The amount of the SiO_2 on the surface was estimated on the Si2p (binding energy 103.4 eV). After 1 month from laser ablation the amount of the SiO_2 was 29.88%, whereas after 5 months 31.21%.

The XRD technique was used to determine the mean size and deviation standard size silver crystallites on a laser-modified silicon surface. It was calculated that 95.45% of the crystallites of silver are between 25.4 nm and 44.8 nm and their average size is 33.8 nm. The size of the crystallites (which usually appear, according the SEM, as agglomerates with size ranging from 60 nm to 100 nm) corresponds to the optimal size of nanostructures (50–70 nm) for the LSPR resonance.

The detailed results and description of XRD and XPS analysis were placed in ESI (Chapter S2).

3.4. *Spectroscopic characterization of the SERS platforms*

3.4.1. *Enhancement factor*

The enhancement factor (EF) is one of the important factors characterizing the spectroscopic properties of SERS-active support. In our work, 10^{-6} M solution of ethanolic *p*-mercaptobenzoic acid (*p*-MBA) was used as a test analyte to evaluate

the sensitivity of our platforms. The details of the calculations of the enhancement factor were presented in Supplementary Materials.

Table S2 summarizes the calculated EFs for all tested and discussed above combinations of parameters used for platform fabrication. As can be seen, our developed method of SERS-active support fabrication delivers a substrate with a very high enhancement factor, ranging from 8.19×10^6 to 3.24×10^8. It was confirmed, that the best parameters for the preparation of the most efficient SERS structures are: fluence 2293 J m^{-2} arrangement of perpendicular scanning layers, substrate scanning speed 1.5 m/s line distance scanning 30 μm, the metal layer 100 nm silver and such fabricated SERS substrates were further used for their reproducibility studies and biological applications.

3.4.2. *Reproducibility and stability*

The reproducibility of recorded spectra and the stability of the SERS platform are essential parameters in biomedical applications of the SERS technique. The high value of the reproducibility is related to the uniform morphology of the platform surface and high density of the 'hot-spots'. Fig. 4a demonstrates two-dimensional SERS spectra recorded in 26 different places over the platform. The similar and high repeatability between individual spectra in the recorded maps was also observed for platforms manufactured in separate processes. The reproducibility of the SERS spectra signal across a single platform was calculated based on the standard deviation method. Calculated standard deviation (SD) for *p*-MBA 10^{-6} M based on the intensity of the band at 1075 cm^{-1} is 4% in relation to the intensity at the same Raman shift of the average plot.

The SERS efficiency was evaluated using the *p*-MBA 10^{-6} M solution for freshly prepared surfaces and those after 3, 4 and 6 months from their manufacture. Fig. 4b exhibits an averaged intensity of the 1075 cm^{-1} band and the corresponding enhancement factor. The EF after 3 months in at the same level as for freshly received platform. The slight decrease of signal and EF can be observed for 4 and 6 months, but EF is still above 10^8, which proves extremely high physical and chemical stability of the proposed SERS platform.

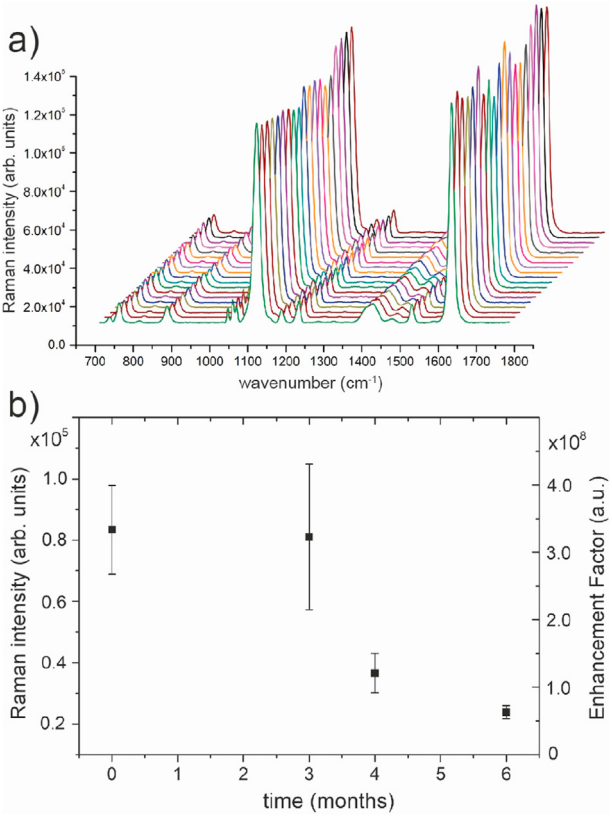

Fig. 4 – (a) The representative two-dimensional SERS spectra of *p*-MBA (10^{-6} M) recorded from 26 different spots on the SERS surface using mapping mode. (b) The stability of the SERS platform with *p*-MBA on the surface within six months from its development. The left axis demonstrates the averaged intensity of the 1075 cm^{-1} band, whereas the right axis demonstrates the enhancement factor (EF) of the platform. The numerical values of b are presented in Table S4.

3.5. *Biological applications*

Candida spp. is the most important opportunistic fungal pathogenic to humans that may cause the oral mucosa, gastrointestinal tract, genitourinary system, vagina, skin infections and many other serious diseases [25–29]. Moreover, it was reported that *Candida* spp. is the most common of the bloodstream infection behind enterococci and staphylococci [30]. However, the mortality rate is significantly higher in the case of *Candida* than *S. aureus* infections [31]. In the case of e.g., vulvovaginal candidiasis (VVC), this infection affects approximately 75% at least once during fertile age and the most responsible species are: *C. albicans* (90% of cases) and *C. glabrata* (10%) [26,32].

In this study, for the first time, we have presented the application of our novel SERS substrates for spectroscopic investigations of these pathogens (*C. glabrata, C. albicans SN148 and C. albicans BWP17*) as well as their chemometric supported differentiation from bacteria *S. aureus* ATCC 29213.

The analysis was completed for *Candida* species growing on two different media: chromogenic medium (CAN2) and YPD medium and *S. aureus* grown on Columbia blood agar. The chromogenic medium consists of a specific substrate that is hydrolyzed by the yeast causes specific staining for unambiguous and rapid identification of yeast. In the case of CAN2 *C. albicans* stains blue, whereas *C. glabrata* grows as white colonies. For each *Candida* species, which were cultured on CAN2 medium obtained spectra along with averaged spectrum marked as black were superimposed and presented in Fig. 5a. As can be noticed, spectra for all of these investigated microorganisms reveal bands which can be assigned to a specific oscillation of biomolecules created an outer structure of them. For instance, the band at 655 cm^{-1} can be assigned to COO^- deformation of amino acids, in turn, the presence of lipids and proteins are indicated by the bands at 1457 cm^{-1} and 957 cm^{-1}, respectively [33–35]. For further analysis of the band's assignments, see Table S5 [36–40]. It should be highlighted that the spectra within a single map are very similar to each other. The similarity means that the novel SERS

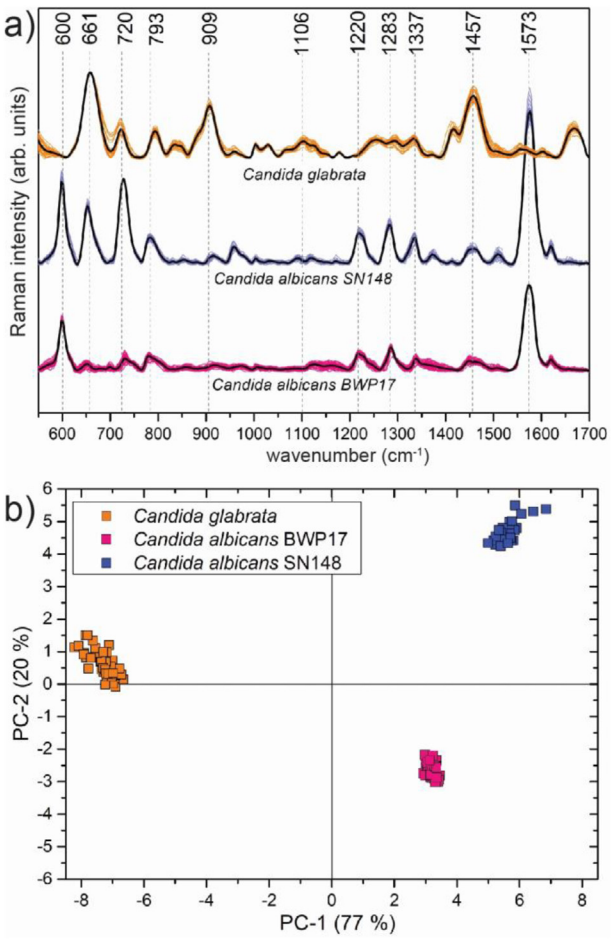

Fig. 5 – (a) The SERS superimposed spectra of maps (orange, blue and pink) and averaged spectra (black) of *Candida glabrata*, *Candida albicans SN148* and *Candida albicans BWP17* cultured on CAN2 medium. For each *Candida* spp. about 50 single spectra were recorded (3 accumulations for 6000 ms each). (b) the PCA scores for *Candida* spp.

substrate provides high repeatability of the SERS signal and its stability during measurements. The calculated standard deviation (SD) for *C. albicans BWP17* based on the intensity of the band at 1457 cm^{-1} is 2.8% in relation to the intensity at the same Raman shift of the average plot.

For better illustration differences among analyzed spectra of microorganisms, Principal Component Analysis was performed over the recorded and preprocessed data. PCA is a chemometric analysis where the mathematical algorithm is based on the reduction of the dimensionality of many complex data. In a new coordinate system, one single spectrum represents a single point [41,42]. Data presented in Fig. 4b reveal the distinct distribution of clusters that are related to spectra of all analyzed *Candida* species cultured on CAN2 medium. The calculated first and the second principal components explain 97% of the total spectral variance and very well divide the group of *C. albicans SN148* and *C. albicans BWP17* from the group of *C. glabrata* and revealed the potential of the SERS technique for strain differentiation of *Candida* species.

Moreover, we have shown the capability of our SERS substrate, supported by the chemometric analysis, to distinguish the *Candida* species from Gram-positive bacterial samples with *S. aureus*. The details of the performed experiment are presented in the Supplementary Materials. The PCA results obtained for this association, namely *C. albicans SN148*, *C. albicans BWP17*, *C. glabrata* and *S. aureus* clearly indicate a good separation of all investigated species (Fig. S15b) and related spectra you can see in Fig. S15a (see ESI).

Remarkably, the calculated scores prove that the first and the second principal components (PC1, PC2) are the most significant and explain 83% of the variance in the data and clearly indicate successful species identification between fungal and bacterial samples. Furthermore, based on the PC-1 loadings, the PCA technique allows us to find the most prominent bands, that strongly influenced obtained differentiation, i.e. 657 cm^{-1}, 835 cm^{-1}, 905 cm^{-1}, 1101 cm^{-1}, 1243 cm^{-1} and 1689 cm^{-1} (Fig. S15c). The most weighted variables, assigned and presented along with their weightings, are nicely correlated with SERS spectra (Figs. S15b and c).

To summarize, species and strain differentiation of pathogenic fungi and bacteria have been demonstrated with our developed SERS substrates.

4. Conclusions

In this paper, we demonstrated a new, versatile SERS platform based on silicon with surface modified with laser ablation. This process was conducted with a femtosecond laser, and therefore, it is fast, cost-effective (in single modification tens of SERS platforms can be produced) and creates a surface without any contaminations. The following parameters of the femtosecond laser modification have been established to achieve the rough and best-enhancing silicon surface: (i) arrangement of scanning layers (perpendicular); (ii) fluence ($E_d = 2293\ J\ m^{-2}$); (iii) beam scanning speed of silicon substrate ($v = 1.5$ m/s); (iv) distance between the scanning lines ($d = 30\ \mu m$), (v) repetition rate ($f = 300$ kHz), (vi) number and pattern of repetitions (double layer is two ablation layers with the mutual orientation of 90°). The influence of the type (Ag, Ag/Au alloys) and the thickness of the deposited onto silicon active metal layers (from 10 nm to 100 nm with a difference of 10 nm) on the SERS efficiency has also been examined. The best result was obtained for 100 nm of the silver layer with the average size of the silver crystallites ranging from 25.4 nm to 44.8 nm, whereas the nanoaggregates are between 60 nm and 100 nm.

The final optimized SERS platform possesses the high enhancement factor at the level of 10^8, extremely high physical and chemical stability for up to 6 months, high reproducibility of SERS responses for both organic and biological analytes the standard deviation (SD) gives 4% for *p*-MBA and 2.8% for *Candida* species, respectively.

We offer the efficient surface-enhanced Raman scattering substrate, which meets all the requirements set for substrates for SERS-based analysis of biomedical samples. Thus our work may open up new opportunities and facilitate biomedical and analytical applications of the SERS method as a routine analysis tool.

Declaration of Competing Interest

The authors declare that they have no known competing financial interests or personal relationships that could have appeared to influence the work reported in this paper.

Acknowledgments

The authors thank for the financial support from the Foundation for Polish Science (FNP) under grant Team-Tech/2017-4/23 (POIR.04.04.00-00-4210/17-00).

Appendix A. Supplementary data

Supplementary data to this article can be found online at https://doi.org/10.1016/j.jmrt.2021.03.083.

REFERENCES

[1] Fleischmann M, Hendra PJ, McQuillan AJ. Raman spectra of pyridine adsorbed at a silver electrode. Chem Phys Lett 1974;26:163–6. https://doi.org/10.1016/0009-2614(74)85388-1.

[2] Le Ru EC, Blackie E, Meyer M, Etchegoint PG. Surface enhanced Raman scattering enhancement factors: a comprehensive study. J Phys Chem C 2007;111:13794–803. https://doi.org/10.1021/jp0687908.

[3] Kneipp K, Wang Y, Kneipp H, Perelman LT, Itzkan I, Dasari RR, et al. Single molecule detection using surface-enhanced Raman scattering (SERS). Phys Rev Lett 1997;78:1667–70. https://doi.org/10.1103/PhysRevLett.78.1667.

[4] Kahraman M, Mullen ER, Korkmaz A, Wachsmann-Hogiu S. Fundamentals and applications of SERS-based bioanalytical sensing. Nanophotonics 2017;6:831–52. https://doi.org/10.1515/nanoph-2016-0174.

[5] Kosuda KM, Bingham JM, Wustholz KL, Van Duyne RP, Groarke RJ. Nanostructures and surface-enhanced Raman spectroscopy. Compr. Nanosci. Nanotechnol. 2019;1–5:117–52. https://doi.org/10.1016/B978-0-12-803581-8.00611-1. Elsevier.

[6] Kamińska A, Dzicielewski I, Weyher JL, Waluk J, Gawinkowski S, Sashuk V, et al. Highly reproducible, stable and multiply regenerated surface-enhanced Raman scattering substrate for biomedical applications. J Mater Chem 2011;21:8662–9. https://doi.org/10.1039/c0jm03336g.

[7] Cyrankiewicz M, Wybranowski T, Kruszewski S. Study of SERS efficiency of metallic colloidal systems. J. Phys. Conf. Ser. 2007;79:012013. https://doi.org/10.1088/1742-6596/79/1/012013. Institute of Physics Publishing.

[8] Liu H, Yang L, Liu J. Three-dimensional SERS hot spots for chemical sensing: towards developing a practical analyzer. TrAC - Trends Anal Chem 2016;80:364–72. https://doi.org/10.1016/j.trac.2015.08.012.

[9] Gattass RR, Mazur E. Femtosecond laser micromachining in transparent materials. Nat Photonics 2008;2:219–25. https://doi.org/10.1038/nphoton.2008.47.

[10] Liu X, Du D, Mourou G. Laser ablation and micromachining with ultrashort laser pulses. IEEE J Quant Electron 1997;33:1706–16. https://doi.org/10.1109/3.631270.

[11] Shirk MD, Molian PA. A review of ultrashort pulsed laser ablation of materials. J Laser Appl 1998;10:18–28. https://doi.org/10.2351/1.521827.

[12] Hamad S, Bharati Moram SS, Yendeti B, Podagatlapalli GK, Nageswara Rao SVS, Pathak AP, et al. Femtosecond laser-induced, nanoparticle-embedded periodic surface structures on crystalline silicon for reproducible and multi-utility SERS platforms. ACS Omega 2018;3:18420–32. https://doi.org/10.1021/acsomega.8b02629.

[13] Saikiran V, Dar MH, Kuladeep R, Desai NR. Ultrafast laser induced subwavelength periodic surface structures on semiconductors/metals and application to SERS studies. MRS Adv 2016;1:3317–27. https://doi.org/10.1557/adv.2016.468. Materials Research Society.

[14] Diebold ED, Mack NH, Doom SK, Mazur E. Femtosecond laser-nanostructured substrates for surface-enhanced Raman scattering. Langmuir 2009;25:1790–4. https://doi.org/10.1021/la803357q.

[15] Wang A, Jiang L, Li X, Xie Q, Li B, Wang Z, et al. Low-adhesive superhydrophobic surface-enhanced Raman spectroscopy substrate fabricated by femtosecond laser ablation for ultratrace molecular detection. J Mater Chem B 2017;5:777–84. https://doi.org/10.1039/c6tb02629j.

[16] Szczepanek J, Kardaś TM, Radzewicz C, Stepanenko Y. Nonlinear polarization evolution of ultrashort pulses in polarization maintaining fibers. Opt Express 2018;26:13590. https://doi.org/10.1364/oe.26.013590.

[17] Kardaś TM, Stepanenko Y, Radzewicz C. Noncollinear and nonlinear pulse propagation. Sci Rep 2018;8:14350. https://doi.org/10.1038/s41598-018-32676-9.

[18] Downer MC, Fork RL, Shank CV. Femtosecond imaging of melting and evaporation at a photoexcited silicon surface. J Opt Soc Am B 1985;2:595. https://doi.org/10.1364/josab.2.000595.

[19] Ionin AA, Kudryashov SI, Samokhin AA. Material surface ablation produced by ultrashort laser pulses. Phys Usp 2017;60:149–60. https://doi.org/10.3367/ufne.2016.09.037974.

[20] Yang J, Li J, Du Z, Gong Q, Teng J, Hong M. Laser hybrid Micro/nano-structuring of Si surfaces in air and its applications for SERS detection. Sci Rep 2014;4. https://doi.org/10.1038/srep06657.

[21] Ravi-Kumar S, Lies B, Zhang X, Lyu H, Qin H. Laser ablation of polymers: a review. Polym Int 2019;68:1391–401. https://doi.org/10.1002/pi.5834.

[22] Ahmmed K, Grambow C, Kietzig A-M. Fabrication of micro/nano structures on metals by femtosecond laser micromachining. Micromachines 2014;5:1219–53. https://doi.org/10.3390/mi5041219.

[23] Borowiec A, Haugen HK. Subwavelength ripple formation on the surfaces of compound semiconductors irradiated with femtosecond laser pulses. Appl Phys Lett 2003;82:4462–4. https://doi.org/10.1063/1.1586457.

[24] Stępak B, Gazińska M, Nejbauer M, Stepanenko Y, Antończak A. Diverse nature of femtosecond laser ablation of poly(L-lactide) and the influence of filamentation on the polymer crystallization behaviour. Sci Rep 2019;9:1–12. https://doi.org/10.1038/s41598-019-39640-1.

[25] Staniszewska M. Virulence factors in Candida species. Curr Protein Pept Sci 2019;21:313–23. https://doi.org/10.2174/1389203720666190722152415.

[26] Naglik JR, Moyes DL. Mucosal immunity and candida albicans infection. Clin Dev Immunol 2011;2011. https://doi.org/10.1155/2011/346307.

[27] Sobel JD. Vulvovaginal candidosiss. Lancet 2007;369:1961–71. https://doi.org/10.1016/S0140-6736(07)60917-9.

[28] Achkar JM, Fries BC. Candida infections of the genitourinary tract. Clin Microbiol Rev 2010;23:253–73. https://doi.org/10.1128/CMR.00076-09.

[29] Coleman DC, Bennett DE, Sullivan DJ, Gallagher PJ, Henman MC, Shanley DB, et al. Oral candida in HIV infection and AIDS: new perspectives/new approaches. Crit Rev Microbiol 1993;19:61–82. https://doi.org/10.3109/10408419309113523.

[30] Wisplinghoff H, Bischoff T, Tallent SM, Seifert H, Wenzel RP, Edmond MB. Nosocomial bloodstream infections in US hospitals: analysis of 24,179 cases from a prospective nationwide surveillance study. Clin Infect Dis 2004;39:309–17. https://doi.org/10.1086/421946.

[31] Gudlaugsson O, Gillespie S, Lee K, Vande Berg J, Hu J, Messer S, et al. Attributable mortality of nosocomial candidemia, revisited. Clin Infect Dis 2003;37:1172–7. https://doi.org/10.1086/378745.

[32] Sobel JD. Key note lecture review article vulvovaginitis due to *Candida glabrata*. an emerging problem. Mycoses 1998;41:18–22. https://doi.org/10.1111/j.1439-0507.1998.tb00594.x.

[33] Wang S, Gu B, Li J, Wang C, Kang H, Shao L, et al. Label-free identification carbapenem-resistant Escherichia coli based on surface-enhanced resonance Raman scattering†. RSC Adv 2018;8:4761–5. https://doi.org/10.1039/c7ra13063e.

[34] Prakash O, Sil S, Verma T, Umapathy S. Direct detection of bacteria using positively charged Ag/Au bimetallic nanoparticles: a label-free surface-enhanced Raman scattering study coupled with multivariate analysis. J Phys Chem C 2020. https://doi.org/10.1021/acs.jpcc.9b09311.

[35] Liu Y, Zhou H, Hu Z, Yu G, Yang D, Zhao J. Label and label-free based surface-enhanced Raman scattering for pathogen bacteria detection: a review. Biosens Bioelectron 2017;94:131–40. https://doi.org/10.1016/j.bios.2017.02.032.

[36] Liang W, Chen Q, Peng F, Shen A, Hu J. A novel surface-enhanced Raman scattering (SERS) detection for natural gas exploration using methane-oxidizing bacteria. Talanta 2018;184:156–61. https://doi.org/10.1016/j.talanta.2018.02.099.

[37] Dina NE, Gherman AMR, Chiş V, Sârbu C, Wieser A, Bauer D, et al. Characterization of clinically relevant fungi via SERS fingerprinting assisted by novel chemometric models. Anal Chem 2018;90:2484–92. https://doi.org/10.1021/acs.analchem.7b03124.

[38] Szeghalmi A, Kaminskyj S, Rösch P, Popp J, Gough KM. Time fluctuations and imaging in the SERS spectra of fungal hypha grown on nanostructured substrates. J Phys Chem B 2007;111:12916–24. https://doi.org/10.1021/jp075422a.

[39] Sayin I, Kahraman M, Sahin F, Yurdakul D, Culha M. Characterization of yeast species using surface-enhanced Raman scattering. Appl Spectrosc 2009;63:1276–82. https://doi.org/10.1366/000370209789806849.

[40] Berus S, Witkowska E, Niciński K, Sadowy E, Puzia W, Ronkiewicz P, et al. Surface-enhanced Raman scattering as a discrimination method of Streptococcus spp. and alternative approach for identifying capsular types of S. pneumoniae isolates. Spectrochim Acta Part A Mol Biomol Spectrosc 2020;233:118088. https://doi.org/10.1016/j.saa.2020.118088.

[41] Ringnér M. What is principal component analysis? Nat Biotechnol 2008;26:303–4. https://doi.org/10.1038/nbt0308-303.

[42] Ding C, He X. *K*-means clustering via principal component analysis. In: Twenty-first int. Conf. Mach. Learn. - icml '04. New York, New York, USA: ACM Press; 2004. p. 29. https://doi.org/10.1145/1015330.1015408.